

Chapter 6

Molecular and Solid State Structure

6.1 Crystal Structure¹

6.1.1 Introduction

In any sort of discussion of crystalline materials, it is useful to begin with a discussion of crystallography: the study of the formation, structure, and properties of crystals. A crystal structure is defined as the particular repeating arrangement of atoms (molecules or ions) throughout a crystal. Structure refers to the internal arrangement of particles and not the external appearance of the crystal. However, these are not entirely independent since the external appearance of a crystal is often related to the internal arrangement. For example, crystals of cubic rock salt (NaCl) are physically cubic in appearance. Only a few of the possible crystal structures are of concern with respect to simple inorganic salts and these will be discussed in detail, however, it is important to understand the nomenclature of crystallography.

6.1.2 Crystallography

6.1.2.1 Bravais lattice

The Bravais lattice is the basic building block from which all crystals can be constructed. The concept originated as a topological problem of finding the number of different ways to arrange points in space where each point would have an identical “atmosphere”. That is each point would be surrounded by an identical set of points as any other point, so that all points would be indistinguishable from each other. Mathematician Auguste Bravais discovered that there were 14 different collections of the groups of points, which are known as Bravais lattices. These lattices fall into seven different “crystal systems”, as differentiated by the relationship between the angles between sides of the “unit cell” and the distance between points in the unit cell. The unit cell is the smallest group of atoms, ions or molecules that, when repeated at regular intervals in three dimensions, will produce the lattice of a crystal system. The “lattice parameter” is the length between two points on the corners of a unit cell. Each of the various lattice parameters are designated by the letters a , b , and c . If two sides are equal, such as in a tetragonal lattice, then the lengths of the two lattice parameters are designated a and c , with b omitted. The angles are designated by the Greek letters α , β , and γ , such that an angle with a specific Greek letter is not subtended by the axis with its Roman equivalent. For example, α is the included angle between the b and c axis.

Table 6.1 shows the various crystal systems, while Figure 6.1 shows the 14 Bravais lattices. It is important to distinguish the characteristics of each of the individual systems. An example of a material that takes on each of the Bravais lattices is shown in Table 6.2.

¹This content is available online at <<http://cnx.org/content/m16927/1.10/>>.

System	Axial lengths and angles	Unit cell geometry
cubic	$a = b = c, \alpha = \beta = \gamma = 90^\circ$	
tetragonal	$a = b \neq c, \alpha = \beta = \gamma = 90^\circ$	
orthorhombic	$a \neq b \neq c, \alpha = \beta = \gamma = 90^\circ$	
rhombohedral	$a = b = c, \alpha = \beta = \gamma \neq 90^\circ$	
hexagonal	$a = b \neq c, \alpha = \beta = 90^\circ, \gamma = 120^\circ$	
monoclinic	$a \neq b \neq c, \alpha = \gamma = 90^\circ, \beta \neq 90^\circ$	
triclinic	$a \neq b \neq c, \alpha \neq \beta \neq \gamma$	

Table 6.1: Geometrical characteristics of the seven crystal systems.

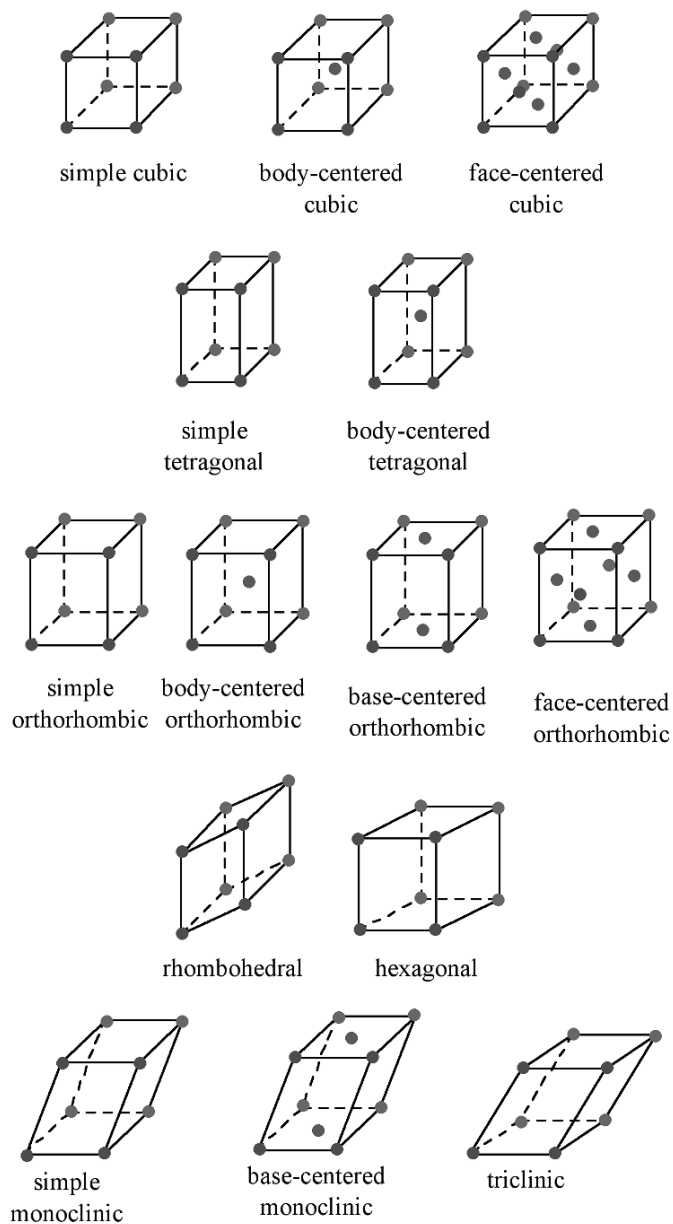


Figure 6.1: Bravais lattices.

Crystal system	Example
triclinic	$\text{K}_2\text{S}_2\text{O}_8$
monoclinic	As_4S_4 , KNO_2
rhombohedral	Hg, Sb
hexagonal	Zn, Co, NiAs
orthorhombic	Ga, Fe_3C
tetragonal	In, TiO_2
cubic	Au, Si, NaCl

Table 6.2: Examples of elements and compounds that adopt each of the crystal systems.

The cubic lattice is the most symmetrical of the systems. All the angles are equal to 90° , and all the sides are of the same length ($a = b = c$). Only the length of one of the sides (a) is required to describe this system completely. In addition to simple cubic, the cubic lattice also includes body-centered cubic and face-centered cubic (Figure 6.1). Body-centered cubic results from the presence of an atom (or ion) in the center of a cube, in addition to the atoms (ions) positioned at the vertices of the cube. In a similar manner, a face-centered cubic requires, in addition to the atoms (ions) positioned at the vertices of the cube, the presence of atoms (ions) in the center of each of the cubes face.

The tetragonal lattice has all of its angles equal to 90° , and has two out of the three sides of equal length ($a = b$). The system also includes body-centered tetragonal (Figure 6.1).

In an orthorhombic lattice all of the angles are equal to 90° , while all of its sides are of unequal length. The system needs only to be described by three lattice parameters. This system also includes body-centered orthorhombic, base-centered orthorhombic, and face-centered orthorhombic (Figure 6.1). A base-centered lattice has, in addition to the atoms (ions) positioned at the vertices of the orthorhombic lattice, atoms (ions) positioned on just two opposing faces.

The rhombohedral lattice is also known as trigonal, and has no angles equal to 90° , but all sides are of equal length ($a = b = c$), thus requiring only by one lattice parameter, and all three angles are equal ($\alpha = \beta = \gamma$).

A hexagonal crystal structure has two angles equal to 90° , with the other angle (γ) equal to 120° . For this to happen, the two sides surrounding the 120° angle must be equal ($a = b$), while the third side (c) is at 90° to the other sides and can be of any length.

The monoclinic lattice has no sides of equal length, but two of the angles are equal to 90° , with the other angle (usually defined as β) being something other than 90° . It is a tilted parallelogram prism with rectangular bases. This system also includes base-centered monoclinic (Figure 6.1).

In the triclinic lattice none of the sides of the unit cell are equal, and none of the angles within the unit cell are equal to 90° . The triclinic lattice is chosen such that all the internal angles are either acute or obtuse. This crystal system has the lowest symmetry and must be described by 3 lattice parameters (a , b , and c) and the 3 angles (α , β , and γ).

6.1.2.2 Atom positions, crystal directions and Miller indices

6.1.2.2.1 Atom positions and crystal axes

The structure of a crystal is defined with respect to a unit cell. As the entire crystal consists of repeating unit cells, this definition is sufficient to represent the entire crystal. Within the unit cell, the atomic arrangement is expressed using coordinates. There are two systems of coordinates commonly in use, which can cause some confusion. Both use a corner of the unit cell as their origin. The first, less-commonly seen system is that of Cartesian or orthogonal coordinates (X , Y , Z). These usually have the units of Angstroms and relate to the distance in each direction between the origin of the cell and the atom. These coordinates may be

manipulated in the same fashion are used with two- or three-dimensional graphs. It is very simple, therefore, to calculate inter-atomic distances and angles given the Cartesian coordinates of the atoms. Unfortunately, the repeating nature of a crystal cannot be expressed easily using such coordinates. For example, consider a cubic cell of dimension 3.52 Å. Pretend that this cell contains an atom that has the coordinates (1.5, 2.1, 2.4). That is, the atom is 1.5 Å away from the origin in the x direction (which coincides with the *a* cell axis), 2.1 Å in the y (which coincides with the *b* cell axis) and 2.4 Å in the z (which coincides with the *c* cell axis). There will be an equivalent atom in the next unit cell along the x-direction, which will have the coordinates (1.5 + 3.52, 2.1, 2.4) or (5.02, 2.1, 2.4). This was a rather simple calculation, as the cell has very high symmetry and so the cell axes, *a*, *b* and *c*, coincide with the Cartesian axes, X, Y and Z. However, consider lower symmetry cells such as triclinic or monoclinic in which the cell axes are not mutually orthogonal. In such cases, expressing the repeating nature of the crystal is much more difficult to accomplish.

Accordingly, atomic coordinates are usually expressed in terms of fractional coordinates, (*x*, *y*, *z*). This coordinate system is coincident with the cell axes (*a*, *b*, *c*) and relates to the position of the atom in terms of the fraction along each axis. Consider the atom in the cubic cell discussion above. The atom was 1.5 Å in the *a* direction away from the origin. As the *a* axis is 3.52 Å long, the atom is $(1.5/3.52)$ or 0.43 of the axis away from the origin. Similarly, it is $(2.1/3.52)$ or 0.60 of the *b* axis and $(2.4/3.52)$ or 0.68 of the *c* axis. The fractional coordinates of this atom are, therefore, (0.43, 0.60, 0.68). The coordinates of the equivalent atom in the next cell over in the *a* direction, however, are easily calculated as this atom is simply 1 unit cell away in *a*. Thus, all one has to do is add 1 to the x coordinate: (1.43, 0.60, 0.68). Such transformations can be performed regardless of the shape of the unit cell. Fractional coordinates, therefore, are used to retain and manipulate crystal information.

6.1.2.2.2 Crystal directions

The designation of the individual vectors within any given crystal lattice is accomplished by the use of whole number multipliers of the lattice parameter of the point at which the vector exits the unit cell. The vector is indicated by the notation [*hkl*], where *h*, *k*, and *l* are reciprocals of the point at which the vector exits the unit cell. The origination of all vectors is assumed defined as [000]. For example, the direction along the *a*-axis according to this scheme would be [100] because this has a component only in the *a*-direction and no component along either the *b* or *c* axial direction. A vector diagonally along the face defined by the *a* and *b* axis would be [110], while going from one corner of the unit cell to the opposite corner would be in the [111] direction. Figure 6.2 shows some examples of the various directions in the unit cell. The crystal direction notation is made up of the lowest combination of integers and represents unit distances rather than actual distances. A [222] direction is identical to a [111], so [111] is used. Fractions are not used. For example, a vector that intercepts the center of the top face of the unit cell has the coordinates *x* = 1/2, *y* = 1/2, *z* = 1. All have to be inversed to convert to the lowest combination of integers (whole numbers); i.e., [221] in Figure 6.2. Finally, all parallel vectors have the same crystal direction, e.g., the four vertical edges of the cell shown in Figure 6.2 all have the crystal direction [*hkl*] = [001].

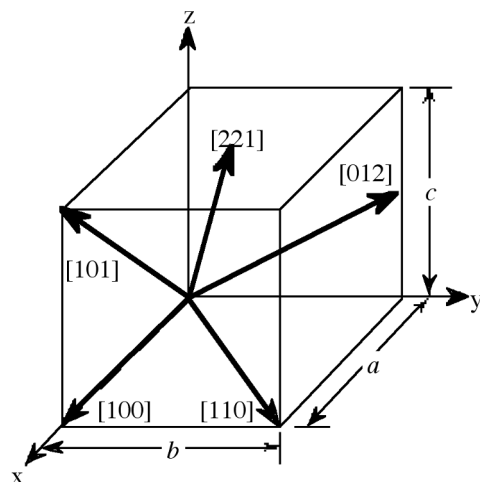


Figure 6.2: Some common directions in a cubic unit cell.

Crystal directions may be grouped in families. To avoid confusion there exists a convention in the choice of brackets surrounding the three numbers to differentiate a crystal direction from a family of direction. For a direction, square brackets $[hkl]$ are used to indicate an individual direction. Angle brackets $\langle hkl \rangle$ indicate a family of directions. A family of directions includes any directions that are equivalent in length and types of atoms encountered. For example, in a cubic lattice, the $[100]$, $[010]$, and $[001]$ directions all belong to the $\langle 100 \rangle$ family of planes because they are equivalent. If the cubic lattice were rotated 90° , the a , b , and c directions would remain indistinguishable, and there would be no way of telling on which crystallographic positions the atoms are situated, so the family of directions is the same. In a hexagonal crystal, however, this is not the case, so the $[100]$ and $[010]$ would both be $\langle 100 \rangle$ directions, but the $[001]$ direction would be distinct. Finally, negative directions are identified with a bar over the negative number instead of a minus sign.

6.1.2.2.3 Crystal planes

Planes in a crystal can be specified using a notation called Miller indices. The Miller index is indicated by the notation $[hkl]$ where h , k , and l are reciprocals of the plane with the x , y , and z axes. To obtain the Miller indices of a given plane requires the following steps:

- Step 1. The plane in question is placed on a unit cell.
- Step 2. Its intercepts with each of the crystal axes are then found.
- Step 3. The reciprocal of the intercepts are taken.
- Step 4. These are multiplied by a scalar to insure that is in the simple ratio of whole numbers.

For example, the face of a lattice that does not intersect the y or z axis would be (100) , while a plane along the body diagonal would be the (111) plane. An illustration of this along with the (111) and (110) planes is given in Figure 6.3.

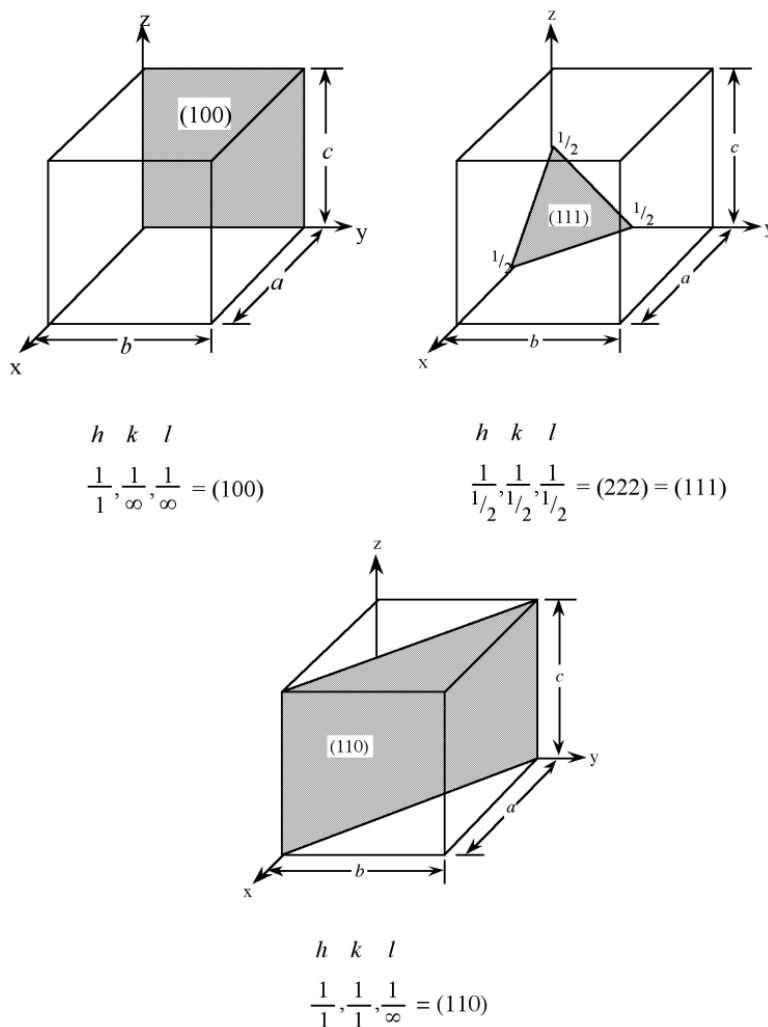


Figure 6.3: Examples of Miller indices notation for crystal planes.

As with crystal directions, Miller indices directions may be grouped in families. Individual Miller indices are given in parentheses (hkl), while braces $\{hkl\}$ are placed around the indices of a family of planes. For example, (001), (100), and (010) are all in the $\{100\}$ family of planes, for a cubic lattice.

6.1.3 Description of crystal structures

Crystal structures may be described in a number of ways. The most common manner is to refer to the size and shape of the unit cell and the positions of the atoms (or ions) within the cell. However, this information is sometimes insufficient to allow for an understanding of the true structure in three dimensions. Consideration of several unit cells, the arrangement of the atoms with respect to each other, the number of other atoms they in contact with, and the distances to neighboring atoms, often will provide a better understanding. A number of methods are available to describe extended solid-state structures. The most applicable with

regard to elemental and compound semiconductor, metals and the majority of insulators is the close packing approach.

6.1.3.1 Close packed structures: hexagonal close packing and cubic close packing

Many crystal structures can be described using the concept of close packing. This concept requires that the atoms (ions) are arranged so as to have the maximum density. In order to understand close packing in three dimensions, the most efficient way for equal sized spheres to be packed in two dimensions must be considered.

The most efficient way for equal sized spheres to be packed in two dimensions is shown in Figure 6.4, in which it can be seen that each sphere (the dark gray shaded sphere) is surrounded by, and is in contact with, six other spheres (the light gray spheres in Figure 6.4). It should be noted that contact with six other spheres the maximum possible is the spheres are the same size, although lower density packing is possible. Close packed layers are formed by repetition to an infinite sheet. Within these close packed layers, three close packed rows are present, shown by the dashed lines in Figure 6.4.

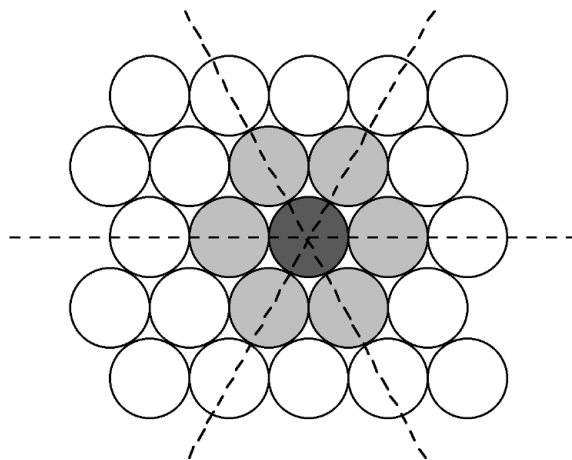


Figure 6.4: Schematic representation of a close packed layer of equal sized spheres. The close packed rows (directions) are shown by the dashed lines.

The most efficient way for equal sized spheres to be packed in three dimensions is to stack close packed layers on top of each other to give a close packed structure. There are two simple ways in which this can be done, resulting in either a hexagonal or cubic close packed structures.

6.1.3.1.1 Hexagonal close packed

If two close packed layers A and B are placed in contact with each other so as to maximize the density, then the spheres of layer B will rest in the hollow (vacancy) between three of the spheres in layer A. This is demonstrated in Figure 6.5. Atoms in the second layer, B (shaded light gray), may occupy one of two possible positions (Figure 6.5a or b) but not both together or a mixture of each. If a third layer is placed on top of layer B such that it exactly covers layer A, subsequent placement of layers will result in the following sequence ...ABABAB.... This is known as hexagonal close packing or *hcp*.

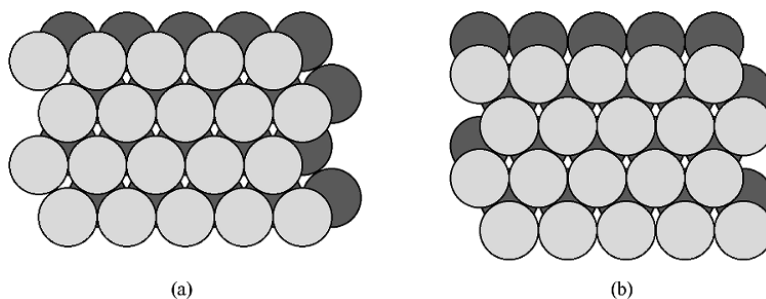


Figure 6.5: Schematic representation of two close packed layers arranged in A (dark grey) and B (light grey) positions. The alternative stacking of the B layer is shown in (a) and (b).

The hexagonal close packed cell is a derivative of the hexagonal Bravais lattice system (Figure 6.1) with the addition of an atom inside the unit cell at the coordinates $(\frac{1}{3}, \frac{2}{3}, \frac{1}{2})$. The basal plane of the unit cell coincides with the close packed layers (Figure 6.6). In other words the close packed layer makes-up the $\{001\}$ family of crystal planes.

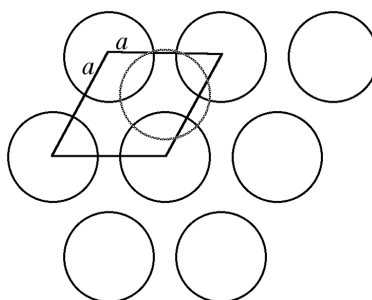


Figure 6.6: A schematic projection of the basal plane of the hcp unit cell on the close packed layers.

The “packing fraction” in a hexagonal close packed cell is 74.05%; that is 74.05% of the total volume is occupied. The packing fraction or density is derived by assuming that each atom is a hard sphere in contact with its nearest neighbors. Determination of the packing fraction is accomplished by calculating the number of whole spheres per unit cell (2 in hcp), the volume occupied by these spheres, and a comparison with the total volume of a unit cell. The number gives an idea of how “open” or filled a structure is. By comparison, the packing fraction for body-centered cubic (Figure 6.1) is 68% and for diamond cubic (an important semiconductor structure to be described later) is 34%.

6.1.3.1.2 Cubic close packed: face-centered cubic

In a similar manner to the generation of the hexagonal close packed structure, two close packed layers are stacked (Figure 6.4) however, the third layer (C) is placed such that it does not exactly cover layer A,

while sitting in a set of troughs in layer B (Figure 6.7), then upon repetition the packing sequence will be ...ABCABCABC.... This is known as cubic close packing or *ccp*.

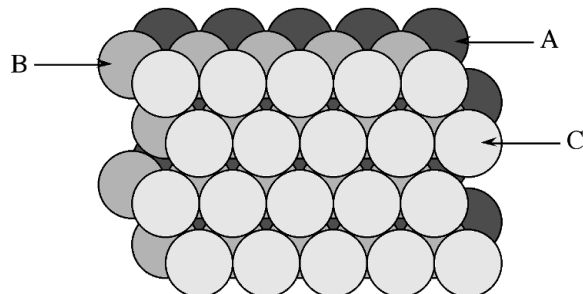


Figure 6.7: Schematic representation of the three close packed layers in a cubic close packed arrangement: A (dark grey), B (medium grey), and C (light grey).

The unit cell of cubic close packed structure is actually that of a face-centered cubic (*fcc*) Bravais lattice. In the *fcc* lattice the close packed layers constitute the $\{111\}$ planes. As with the *hcp* lattice packing fraction in a cubic close packed (*fcc*) cell is 74.05%. Since face centered cubic or *fcc* is more commonly used in preference to cubic close packed (*ccp*) in describing the structures, the former will be used throughout this text.

6.1.3.2 Coordination number

The coordination number of an atom or ion within an extended structure is defined as the number of nearest neighbor atoms (ions of opposite charge) that are in contact with it. A slightly different definition is often used for atoms within individual molecules: the number of donor atoms associated with the central atom or ion. However, this distinction is rather artificial, and both can be employed.

The coordination numbers for metal atoms in a molecule or complex are commonly 4, 5, and 6, but all values from 2 to 9 are known and a few examples of higher coordination numbers have been reported. In contrast, common coordination numbers in the solid state are 3, 4, 6, 8, and 12. For example, the atom in the center of body-centered cubic lattice has a coordination number of 8, because it touches the eight atoms at the corners of the unit cell, while an atom in a simple cubic structure would have a coordination number of 6. In both *fcc* and *hcp* lattices each of the atoms have a coordination number of 12.

6.1.3.3 Octahedral and tetrahedral vacancies

As was mentioned above, the packing fraction in both *fcc* and *hcp* cells is 74.05%, leaving 25.95% of the volume unfilled. The unfilled lattice sites (interstices) between the atoms in a cell are called interstitial sites or vacancies. The shape and relative size of these sites is important in controlling the position of additional atoms. In both *fcc* and *hcp* cells most of the space within these atoms lies within two different sites known as octahedral sites and tetrahedral sites. The difference between the two lies in their “coordination number”, or the number of atoms surrounding each site. Tetrahedral sites (vacancies) are surrounded by four atoms arranged at the corners of a tetrahedron. Similarly, octahedral sites are surrounded by six atoms which make-up the apices of an octahedron. For a given close packed lattice an octahedral vacancy will be larger than a tetrahedral vacancy.

Within a face centered cubic lattice, the eight tetrahedral sites are positioned within the cell, at the general fractional coordinate of $(n/4, n/4, n/4)$ where $n = 1$ or 3 , e.g., $(1/4, 1/4, 1/4)$, $(1/4, 1/4, 3/4)$, etc. The

octahedral sites are located at the center of the unit cell ($1/2, 1/2, 1/2$), as well as at each of the edges of the cell, e.g., ($1/2, 0, 0$). In the hexagonal close packed system, the tetrahedral sites are at ($0, 0, 3/8$) and ($1/3, 2/3, 7/8$), and the octahedral sites are at ($1/3, 1/3, 1/4$) and all symmetry equivalent positions.

6.1.3.4 Important structure types

The majority of crystalline materials do not have a structure that fits into the one atom per site simple Bravais lattice. A number of other important crystal structures are found, however, only a few of these crystal structures are those of which occur for the elemental and compound semiconductors and the majority of these are derived from *fcc* or *hcp* lattices. Each structural type is generally defined by an archetype, a material (often a naturally occurring mineral) which has the structure in question and to which all the similar materials are related. With regard to commonly used elemental and compound semiconductors the important structures are diamond, zinc blende, Wurtzite, and to a lesser extent chalcopyrite. However, rock salt, β -tin, cinnabar and cesium chloride are observed as high pressure or high temperature phases and are therefore also discussed. The following provides a summary of these structures. Details of the full range of solid-state structures are given elsewhere.

6.1.3.4.1 Diamond Cubic

The diamond cubic structure consists of two interpenetrating face-centered cubic lattices, with one offset $1/4$ of a cube along the cube diagonal. It may also be described as face centered cubic lattice in which half of the tetrahedral sites are filled while all the octahedral sites remain vacant. The diamond cubic unit cell is shown in Figure 6.8. Each of the atoms (e.g., C) is four coordinate, and the shortest interatomic distance (C-C) may be determined from the unit cell parameter (a).

$$\text{C-C} = \frac{a\sqrt{3}}{4} \approx 0.422 a \quad (6.1)$$

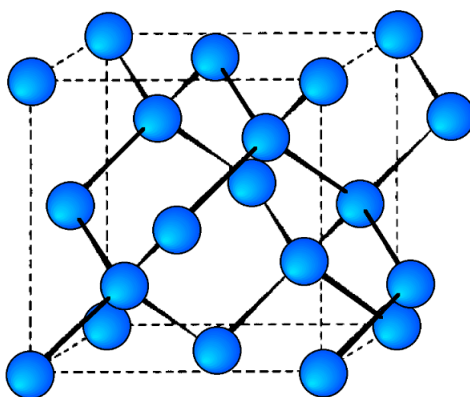


Figure 6.8: Unit cell structure of a diamond cubic lattice showing the two interpenetrating face-centered cubic lattices.

6.1.3.4.2 Zinc blende

This is a binary phase (ME) and is named after its archetype, a common mineral form of zinc sulfide (ZnS). As with the diamond lattice, zinc blende consists of the two interpenetrating *fcc* lattices. However, in zinc blende one lattice consists of one of the types of atoms (Zn in ZnS), and the other lattice is of the second type of atom (S in ZnS). It may also be described as face centered cubic lattice of S atoms in which half of the tetrahedral sites are filled with Zn atoms. All the atoms in a zinc blende structure are 4-coordinate. The zinc blende unit cell is shown in Figure 6.9. A number of inter-atomic distances may be calculated for any material with a zinc blende unit cell using the lattice parameter (a).

$$\text{Zn-S} = \frac{a\sqrt{3}}{4} \approx 0.422 a \quad (6.2)$$

$$\text{Zn-Zn} = \text{S-S} = \frac{a}{\sqrt{2}} \approx 0.707 a \quad (6.3)$$

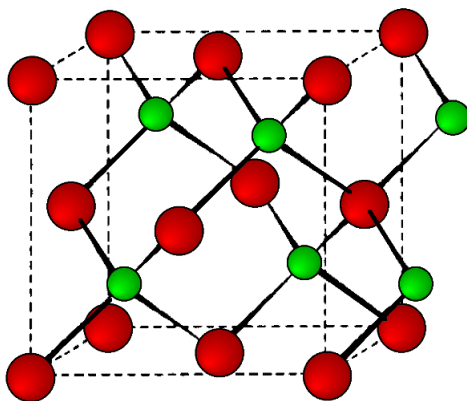


Figure 6.9: Unit cell structure of a zinc blende (ZnS) lattice. Zinc atoms are shown in green (small), sulfur atoms shown in red (large), and the dashed lines show the unit cell.

6.1.3.4.3 Chalcopyrite

The mineral chalcopyrite CuFeS_2 is the archetype of this structure. The structure is tetragonal ($a = b \neq c$, $\alpha = \beta = \gamma = 90^\circ$), and is essentially a superlattice on that of zinc blende. Thus, it is easiest to imagine that the chalcopyrite lattice is made-up of a lattice of sulfur atoms in which the tetrahedral sites are filled in layers, ...FeCuCuFe..., etc. (Figure 6.10). In such an idealized structure $c = 2a$, however, this is not true of all materials with chalcopyrite structures.

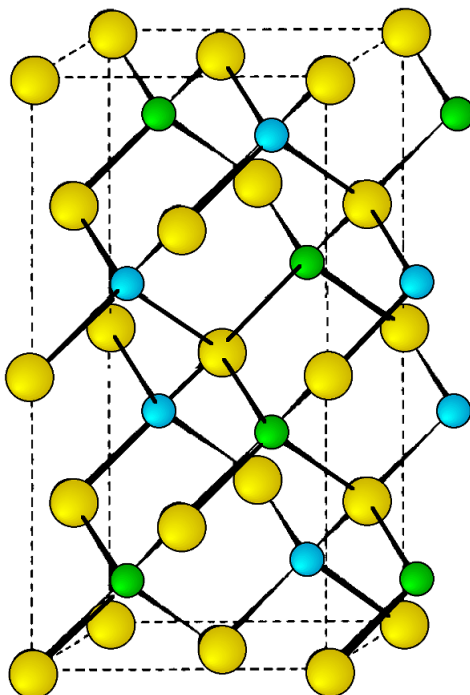


Figure 6.10: Unit cell structure of a chalcopyrite lattice. Copper atoms are shown in blue, iron atoms are shown in green and sulfur atoms are shown in yellow. The dashed lines show the unit cell.

6.1.3.4.4 Rock salt

As its name implies the archetypal rock salt structure is NaCl (table salt). In common with the zinc blende structure, rock salt consists of two interpenetrating face-centered cubic lattices. However, the second lattice is offset $1/2a$ along the unit cell axis. It may also be described as face centered cubic lattice in which all of the octahedral sites are filled, while all the tetrahedral sites remain vacant, and thus each of the atoms in the rock salt structure are 6-coordinate. The rock salt unit cell is shown in Figure 6.11. A number of inter-atomic distances may be calculated for any material with a rock salt structure using the lattice parameter (a).

$$\text{Na-Cl} = \frac{a}{2} \approx 0.5 a \quad (6.4)$$

$$\text{Na-Na} = \text{Cl-Cl} = \frac{a}{\sqrt{2}} \approx 0.707 a \quad (6.5)$$

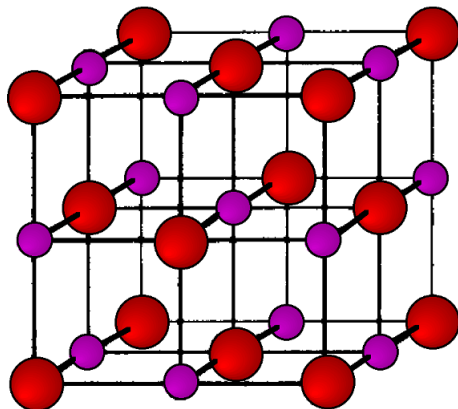


Figure 6.11: Unit cell structure of a rock salt lattice. Sodium ions are shown in purple (small spheres) and chloride ions are shown in red (large spheres).

6.1.3.4.5 Cinnabar

Cinnabar, named after the archetype mercury sulfide, HgS , is a distorted rock salt structure in which the resulting cell is rhombohedral (trigonal) with each atom having a coordination number of six.

6.1.3.4.6 Wurtzite

This is a hexagonal form of the zinc sulfide. It is identical in the number of and types of atoms, but it is built from two interpenetrating *hcp* lattices as opposed to the *fcc* lattices in zinc blende. As with zinc blende all the atoms in a wurtzite structure are 4-coordinate. The wurtzite unit cell is shown in Figure 6.12. A number of inter atomic distances may be calculated for any material with a wurtzite cell using the lattice parameter (a).

$$\text{Zn-S} = a\sqrt{3}/8 = 0.612 a = \frac{3c}{8} = 0.375 c \quad (6.6)$$

$$\text{Zn-Zn} = \text{S-S} = a = 1.632 c \quad (6.7)$$

However, it should be noted that these formulae do not necessarily apply when the ratio a/c is different from the ideal value of 1.632.

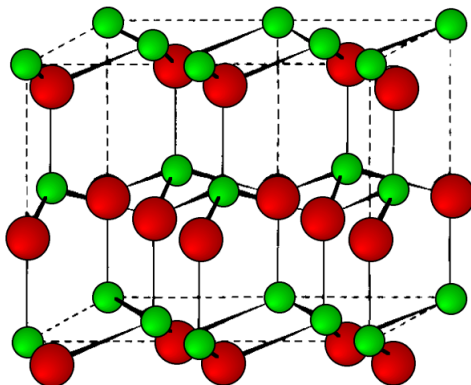


Figure 6.12: Unit cell structure of a wurtzite lattice. Zinc atoms are shown in green (small spheres), sulfur atoms shown in red (large spheres), and the dashed lines show the unit cell.

6.1.3.4.7 Cesium Chloride

The cesium chloride structure is found in materials with large cations and relatively small anions. It has a simple (primitive) cubic cell (Figure 6.1) with a chloride ion at the corners of the cube and the cesium ion at the body center. The coordination numbers of both Cs^+ and Cl^- , with the inner atomic distances determined from the cell lattice constant (a).

$$\text{Cs-Cl} = \frac{a\sqrt{3}}{2} \approx 0.866 a \quad (6.8)$$

$$\text{Cs-Cs} = \text{Cl-Cl} = a \quad (6.9)$$

6.1.3.4.8 β -Tin.

The room temperature allotrope of tin is β -tin or white tin. It has a tetragonal structure, in which each tin atom has four nearest neighbors ($\text{Sn-Sn} = 3.016 \text{ \AA}$) arranged in a very flattened tetrahedron, and two next nearest neighbors ($\text{Sn-Sn} = 3.175 \text{ \AA}$). The overall structure of β -tin consists of fused hexagons, each being linked to its neighbor via a four-membered Sn_4 ring.

6.1.4 Defects in crystalline solids

Up to this point we have only been concerned with ideal structures for crystalline solids in which each atom occupies a designated point in the crystal lattice. Unfortunately, defects ordinarily exist in equilibrium between the crystal lattice and its environment. These defects are of two general types: point defects and extended defects. As their names imply, point defects are associated with a single crystal lattice site, while extended defects occur over a greater range.

6.1.4.1 Point defects: “too many or too few” or “just plain wrong”

Point defects have a significant effect on the properties of a semiconductor, so it is important to understand the classes of point defects and the characteristics of each type. Figure 6.13 summarizes various classes of native point defects, however, they may be divided into two general classes; defects with the wrong number of atoms (deficiency or surplus) and defects where the identity of the atoms is incorrect.

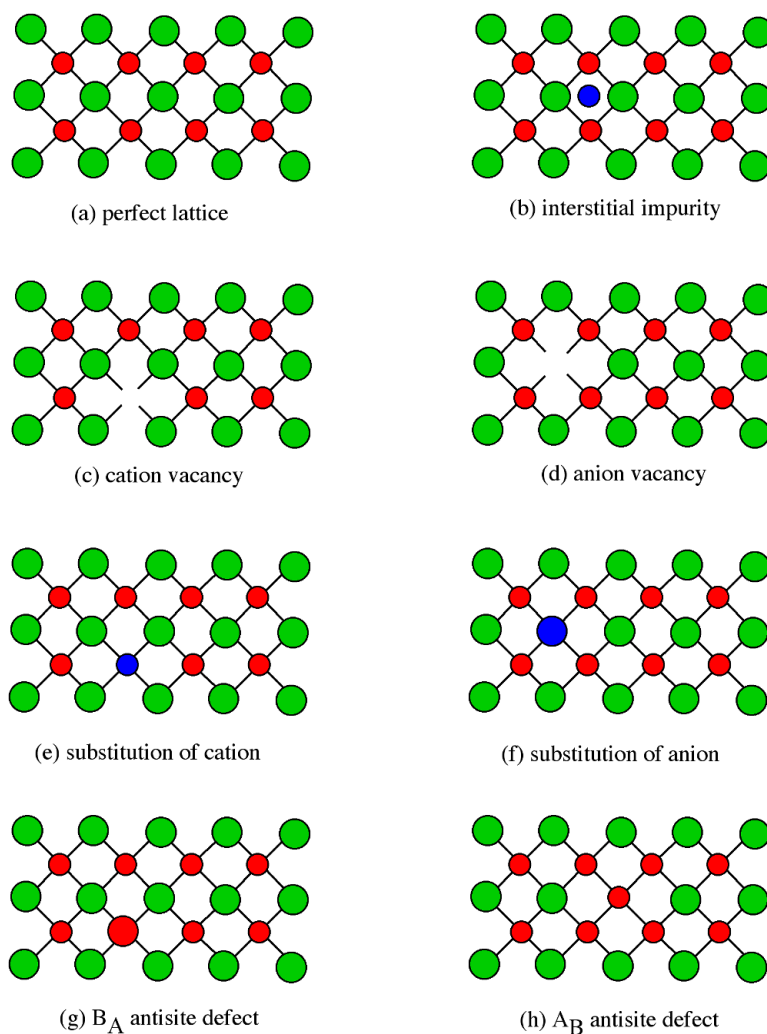


Figure 6.13: Point defects in a crystal lattice.

6.1.4.1.1 Interstitial Impurity

An interstitial impurity occurs when an extra atom is positioned in a lattice site that should be vacant in an ideal structure (Figure 6.13b). Since all the adjacent lattice sites are filled the additional atom will have to squeeze itself into the interstitial site, resulting in distortion of the lattice and alteration in the local

electronic behavior of the structure. Small atoms, such as carbon, will prefer to occupy these interstitial sites. Interstitial impurities readily diffuse through the lattice via interstitial diffusion, which can result in a change of the properties of a material as a function of time. Oxygen impurities in silicon generally are located as interstitials.

6.1.4.1.2 Vacancies

The converse of an interstitial impurity is when there are not enough atoms in a particular area of the lattice. These are called vacancies. Vacancies exist in any material above absolute zero and increase in concentration with temperature. In the case of compound semiconductors, vacancies can be either cation vacancies (Figure 6.13c) or anion vacancies (Figure 6.13d), depending on what type of atom are “missing”.

6.1.4.1.3 Substitution

Substitution of various atoms into the normal lattice structure is common, and used to change the electronic properties of both compound and elemental semiconductors. Any impurity element that is incorporated during crystal growth can occupy a lattice site. Depending on the impurity, substitution defects can greatly distort the lattice and/or alter the electronic structure. In general, cations will try to occupy cation lattice sites (Figure 6.13e), and anion will occupy the anion site (Figure 6.13f). For example, a zinc impurity in GaAs will occupy a gallium site, if possible, while a sulfur, selenium and tellurium atoms would all try to substitute for an arsenic. Some impurities will occupy either site indiscriminately, e.g., Si and Sn occupy both Ga and As sites in GaAs.

6.1.4.1.4 Antisite Defects

Antisite defects are a particular form of substitution defect, and are unique to compound semiconductors. An antisite defect occurs when a cation is misplaced on an anion lattice site or vice versa (Figure 6.13g and h). Depending on the arrangement these are designated as either A_B antisite defects or B_A antisite defects. For example, if an arsenic atom is on a gallium lattice site the defect would be an As_{Ga} defect. Antisite defects involve fitting into a lattice site atoms of a different size than the rest of the lattice, and therefore this often results in a localized distortion of the lattice. In addition, cations and anions will have a different number of electrons in their valence shells, so this substitution will alter the local electron concentration and the electronic properties of this area of the semiconductor.

6.1.4.2 Extended Defects: Dislocations in a Crystal Lattice

Extended defects may be created either during crystal growth or as a consequence of stress in the crystal lattice. The plastic deformation of crystalline solids does not occur such that all bonds along a plane are broken and reformed simultaneously. Instead, the deformation occurs through a dislocation in the crystal lattice. Figure 6.14 shows a schematic representation of a dislocation in a crystal lattice. Two features of this type of dislocation are the presence of an extra crystal plane, and a large void at the dislocation core. Impurities tend to segregate to the dislocation core in order to relieve strain from their presence.

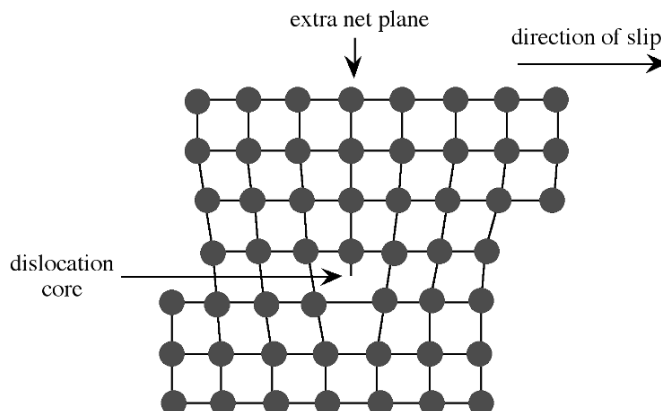


Figure 6.14: Dislocation in a crystal lattice.

6.1.5 Epitaxy

Epitaxy, is a transliteration of two Greek words *epi*, meaning "upon", and *taxis*, meaning "ordered". With respect to crystal growth it applies to the process of growing thin crystalline layers on a crystal substrate. In epitaxial growth, there is a precise crystal orientation of the film in relation to the substrate. The growth of epitaxial films can be done by a number of methods including molecular beam epitaxy, atomic layer epitaxy, and chemical vapor deposition, all of which will be described later.

Epitaxy of the same material, such as a gallium arsenide film on a gallium arsenide substrate, is called homoepitaxy, while epitaxy where the film and substrate material are different is called heteroepitaxy. Clearly, in homoepitaxy, the substrate and film will have the identical structure, however, in heteroepitaxy, it is important to employ where possible a substrate with the same structure and similar lattice parameters. For example, zinc selenide (zinc blende, $a = 5.668 \text{ \AA}$) is readily grown on gallium arsenide (zinc blende, $a = 5.653 \text{ \AA}$). Alternatively, epitaxial crystal growth can occur where there exists a simple relationship between the structures of the substrate and crystal layer, such as is observed between Al_2O_3 (100) on Si (100). Whichever route is chosen a close match in the lattice parameters is required, otherwise, the strains induced by the lattice mismatch results in distortion of the film and formation of dislocations. If the mismatch is significant epitaxial growth is not energetically favorable, causing a textured film or polycrystalline untextured film to be grown. As a general rule of thumb, epitaxy can be achieved if the lattice parameters of the two materials are within about 5% of each other. For good quality epitaxy, this should be less than 1%. The larger the mismatch, the larger the strain in the film. As the film gets thicker and thicker, it will try to relieve the strain in the film, which could include the loss of epitaxy or the growth of dislocations. It is important to note that the $\langle 100 \rangle$ directions of a film must be parallel to the $\langle 100 \rangle$ direction of the substrate. In some cases, such as Fe on MgO, the [111] direction is parallel to the substrate [100]. The epitaxial relationship is specified by giving first the plane in the film that is parallel to the substrate [100].

6.1.6 Bibliography

- *International Tables for X-ray Crystallography*. Vol. IV; Kynoch Press: Birmingham, UK (1974).
- B. F. G. Johnson, in *Comprehensive Inorganic Chemistry*, Pergamon Press, Vol. 4, Chapter 52 (1973).
- A. R. West, *Solid State Chemistry and its Applications*, Wiley, New York (1984).

6.2 Structures of Element and Compound Semiconductors²

6.2.1 Introduction

A single crystal of either an elemental (e.g., silicon) or compound (e.g., gallium arsenide) semiconductor forms the basis of almost all semiconductor devices. The ability to control the electronic and opto-electronic properties of these materials is based on an understanding of their structure. In addition, the metals and many of the insulators employed within a microelectronic device are also crystalline.

6.2.2 Group IV (14) elements

Each of the semiconducting phases of the group IV (14) elements, C (diamond), Si, Ge, and α -Sn, adopt the diamond cubic structure (Figure 6.15). Their lattice constants (a , Å) and densities (ρ , g/cm³) are given in Table 6.3.

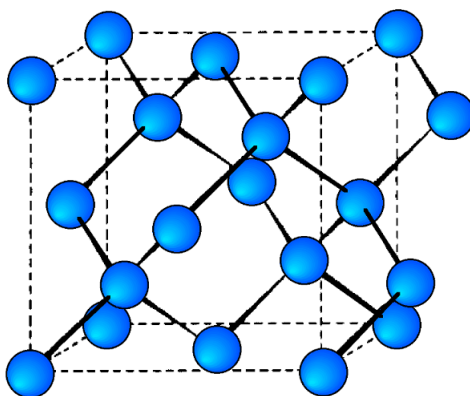


Figure 6.15: Unit cell structure of a diamond cubic lattice showing the two interpenetrating face-centered cubic lattices.

Element	Lattice parameter, a (Å)	Density (g/cm ³)
carbon (diamond)	3.56683(1)	3.51525
silicon	5.4310201(3)	2.319002
germanium	5.657906(1)	5.3234
tin (α -Sn)	6.4892(1)	7.285

Table 6.3: Lattice parameters and densities (measured at 298 K) for the diamond cubic forms of the group IV (14) elements.

As would be expected the lattice parameter increase in the order $C < Si < Ge < \alpha$ -Sn. Silicon and germanium form a continuous series of solid solutions with gradually varying parameters. It is worth noting the high degree of accuracy that the lattice parameters are known for high purity crystals of these elements. In addition, it is important to note the temperature at which structural measurements are made, since the

²This content is available online at <<http://cnx.org/content/m23905/1.6/>>.

lattice parameters are temperature dependent (Figure 6.16). The lattice constant (a), in Å, for high purity silicon may be calculated for any temperature (T) over the temperature range 293 - 1073 K by the formula shown below.

$$a_T = 5.4304 + 1.8138 \times 10^{-5} (T - 298.15 \text{ K}) + 1.542 \times 10^{-9} (T - 298.15 \text{ K})^2$$

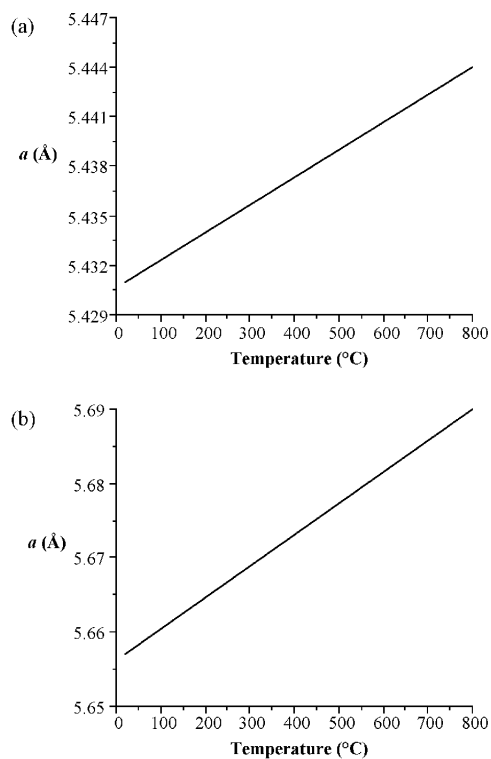


Figure 6.16: Temperature dependence of the lattice parameter for (a) Si and (b) Ge.

Even though the diamond cubic forms of Si and Ge are the only forms of direct interest to semiconductor devices, each exists in numerous crystalline high pressure and meta-stable forms. These are described along with their interconversions, in Table 6.4.

Phase	Structure	Remarks
Si I	diamond cubic	stable at normal pressure
Si II	grey tin structure	formed from Si I or Si V above 14 GPa
Si III	cubic	metastable, formed from Si II above 10 GPa
Si IV	hexagonal	
Si V	unidentified	stable above 34 GPa, formed from Si II above 16 GPa
Si VI	hexagonal close packed	stable above 45 GPa
Ge I	diamond cubic	low-pressure phase
Ge II	β -tin structure	formed from Ge I above 10 GPa
Ge III	tetragonal	formed by quenching Ge II at low pressure
Ge IV	body centered cubic	formed by quenching Ge II to 1 atm at 200 K

Table 6.4: High pressure and metastable phases of silicon and germanium.

6.2.3 Group III-V (13-15) compounds

The stable phases for the arsenides, phosphides and antimonides of aluminum, gallium and indium all exhibit zinc blende structures (Figure 6.17). In contrast, the nitrides are found as wurtzite structures (e.g., Figure 6.18). The structure, lattice parameters, and densities of the III-V compounds are given in Table 6.5. It is worth noting that contrary to expectation the lattice parameter of the gallium compounds is smaller than their aluminum homolog; for GaAs $a = 5.653 \text{ \AA}$; AlAs $a = 5.660 \text{ \AA}$. As with the group IV elements the lattice parameters are highly temperature dependent; however, additional variation arises from any deviation from absolute stoichiometry. These effects are shown in Figure 6.19.

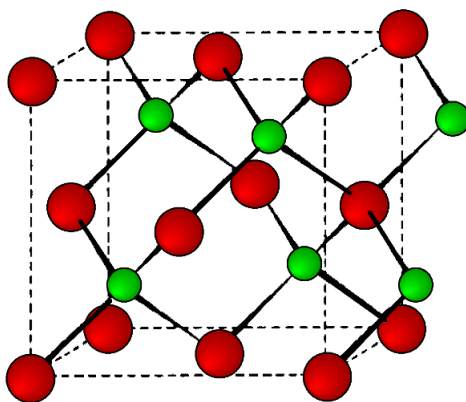


Figure 6.17: Unit cell structure of a zinc blende (ZnS) lattice. Zinc atoms are shown in green (small), sulfur atoms shown in red (large), and the dashed lines show the unit cell.

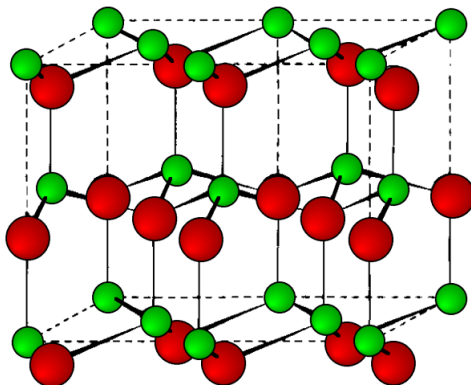


Figure 6.18: Unit cell structure of a wurtzite lattice. Zinc atoms are shown in green (small), sulfur atoms shown in red (large), and the dashed lines show the unit cell.

Compound	Structure	Lattice parameter (Å)	Density (g/cm ³)
AlN	wurtzite	$a = 3.11(1), c = 4.98(1)$	3.255
AlP	zinc blende	$a = 5.4635(4)$	2.40(1)
AlAs	zinc blende	$a = 5.660$	3.760
AlSb	zinc blende	$a = 6.1355(1)$	4.26
GaN	wurtzite	$a = 3.190, c = 5.187$	
GaP	zinc blende	$a = 5.4505(2)$	4.138
GaAs	zinc blende	$a = 5.65325(2)$	5.3176(3)
InN	wurtzite	$a = 3.5446, c = 5.7034$	6.81
InP	zinc blende	$a = 5.868(1)$	4.81
InAs	zinc blende	$a = 6.0583$	5.667
InSb	zinc blende	$a = 6.47937$	5.7747(4)

Table 6.5: Lattice parameters and densities (measured at 298 K) for the III-V (13-15) compound semiconductors. Estimated standard deviations given in parentheses.

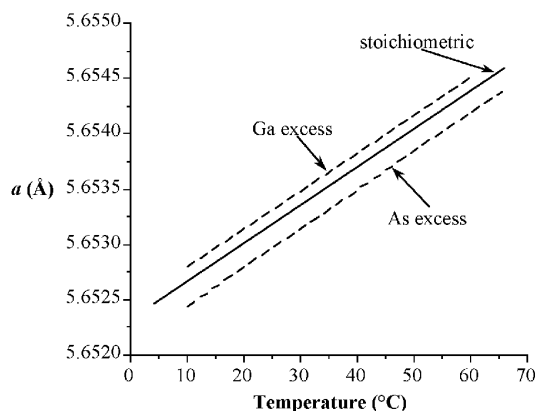


Figure 6.19: Temperature dependence of the lattice parameter for stoichiometric GaAs and crystals with either Ga or As excess.

The homogeneity of structures of alloys for a wide range of solid solutions to be formed between III-V compounds in almost any combination. Two classes of ternary alloys are formed: $\text{III}_x\text{-III}_{1-x}\text{-V}$ (e.g., $\text{Al}_x\text{-Ga}_{1-x}\text{-As}$) and $\text{III-V}_{1-x}\text{-V}_x$ (e.g., $\text{Ga-As}_{1-x}\text{-P}_x$). While quaternary alloys of the type $\text{III}_x\text{-III}_{1-x}\text{-V}_y\text{-V}_{1-y}$ allow for the growth of materials with similar lattice parameters, but a broad range of band gaps. A very important ternary alloy, especially in optoelectronic applications, is $\text{Al}_x\text{-Ga}_{1-x}\text{-As}$ and its lattice parameter (a) is directly related to the composition (x).

$$a = 5.6533 + 0.0078 x$$

Not all of the III-V compounds have well characterized high-pressure phases. However, in each case where a high-pressure phase is observed the coordination number of both the group III and group V element increases from four to six. Thus, AlP undergoes a zinc blende to rock salt transformation at high pressure above 170 kbar, while AlSb and GaAs form orthorhombic distorted rock salt structures above 77 and 172 kbar, respectively. An orthorhombic structure is proposed for the high-pressure form of InP (>133 kbar). Indium arsenide (InAs) undergoes two-phase transformations. The zinc blende structure is converted to a rock salt structure above 77 kbar, which in turn forms a β -tin structure above 170 kbar.

6.2.4 Group II-VI (12-16) compounds

The structures of the II-VI compound semiconductors are less predictable than those of the III-V compounds (above), and while zinc blende structure exists for almost all of the compounds there is a stronger tendency towards the hexagonal wurtzite form. In several cases the zinc blende structure is observed under ambient conditions, but may be converted to the wurtzite form upon heating. In general the wurtzite form predominates with the smaller anions (e.g., oxides), while the zinc blende becomes the more stable phase for the larger anions (e.g., tellurides). One exception is mercury sulfide (HgS) that is the archetype for the trigonal cinnabar phase. Table 6.6 lists the stable phase of the chalcogenides of zinc, cadmium and mercury, along with their high temperature phases where applicable. Solid solutions of the II-VI compounds are not as easily formed as for the III-V compounds; however, two important examples are $\text{ZnS}_x\text{Se}_{1-x}$ and $\text{Cd}_x\text{Hg}_{1-x}\text{Te}$.

Compound	Structure	Lattice parameter (Å)	Density (g/cm ³)
ZnS	zinc blende	$a = 5.410$	4.075
	wurtzite	$a = 3.822, c = 6.260$	4.087
ZnSe	Zinc blende	$a = 5.668$	5.27
ZnTe	Zinc blende	$a = 6.10$	5.636
CdS	wurtzite	$a = 4.136, c = 6.714$	4.82
CdSe	wurtzite	$a = 4.300, c = 7.011$	5.81
CdTe	Zinc blende	$a = 6.482$	5.87
HgS	cinnabar	$a = 4.149, c = 9.495$	
	Zinc blende	$a = 5.851$	7.73
HgSe	Zinc blende	$a = 6.085$	8.25
HgTe	Zinc blende	$a = 6.46$	8.07

Table 6.6: Lattice parameters and densities (measured at 298 K) for the II-VI (12-16) compound semiconductors.

The zinc chalcogenides all transform to a cesium chloride structure under high pressures, while the cadmium compounds all form rock salt high-pressure phases (Figure 6.20). Mercury selenide (HgSe) and mercury telluride (HgTe) convert to the mercury sulfide archetype structure, cinnabar, at high pressure.

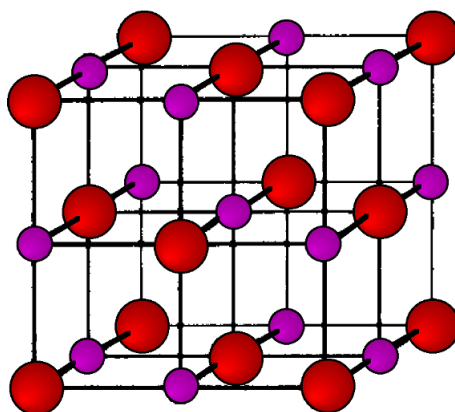


Figure 6.20: Unit cell structure of a rock salt lattice. Sodium ions are shown in purple and chloride ions are shown in red.

6.2.5 I-III-VI₂ (11-13-16) compounds

Nearly all I-III-VI₂ compounds at room temperature adopt the chalcopyrite structure (Figure 6.21). The cell constants and densities are given in Table 6.7. Although there are few reports of high temperature or

high-pressure phases, AgInS_2 has been shown to exist as a high temperature orthorhombic polymorph ($a = 6.954$, $b = 8.264$, and $c = 6.683 \text{ \AA}$), and AgInTe_2 forms a cubic phase at high pressures.

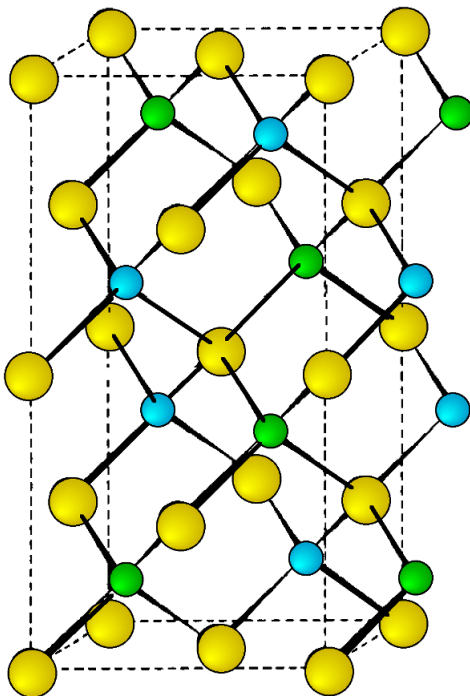


Figure 6.21: Unit cell structure of a chalcopyrite lattice. Copper atoms are shown in blue, iron atoms are shown in green and sulfur atoms are shown in yellow. The dashed lines show the unit cell.

Compound	Lattice parameter a (Å)	Lattice parameter c (Å)	Density (g.cm ³)
CuAlS ₂	5.32	10.430	3.45
CuAlSe ₂	5.61	10.92	4.69
CuAlTe ₂	5.96	11.77	5.47
CuGaS ₂	5.35	10.46	4.38
CuGaSe ₂	5.61	11.00	5.57
CuGaTe ₂	6.00	11.93	5.95
CuInS ₂	5.52	11.08	4.74
CuInSe ₂	5.78	11.55	5.77
CuInTe ₂	6.17	12.34	6.10
AgAlS ₂	6.30	11.84	6.15
AgGaS ₂	5.75	10.29	4.70
AgGaSe ₂	5.98	10.88	5.70
AgGaTe ₂	6.29	11.95	6.08
AgInS ₂	5.82	11.17	4.97
AgInSe ₂	6.095	11.69	5.82
AgInTe ₂	6.43	12.59	6.96

Table 6.7: Chalcopyrite lattice parameters and densities (measured at 298 K) for the I-III-VI compound semiconductors. Lattice parameters for tetragonal cell.

Of the I-III-VI₂ compounds, the copper indium chalcogenides (CuInE₂) are certainly the most studied for their application in solar cells. One of the advantages of the copper indium chalcogenide compounds is the formation of solid solutions (alloys) of the formula CuInE_{2-x}E'_x, where the composition variable (x) varies from 0 to 2. The CuInS_{2-x}Se_x and CuInSe_{2-x}Te_x systems have also been examined, as has the CuGa_yIn_{1-y}S_{2-x}Se_x quaternary system. As would be expected from a consideration of the relative ionic radii of the chalcogenides the lattice parameters of the CuInS_{2-x}Se_x alloy should increase with increased selenium content. Vegard's law requires the lattice constant for a linear solution of two semiconductors to vary linearly with composition (e.g., as is observed for Al_xGa_{1-x}As), however, the variation of the tetragonal lattice constants (a and c) with composition for CuInS_{2-x}S_x are best described by the parabolic relationships.

$$a = 5.532 + 0.0801 x + 0.0260 x^2$$

$$c = 11.156 + 0.1204 x + 0.0611 x^2$$

A similar relationship is observed for the CuInSe_{2-x}Te_x alloys.

$$a = 5.783 + 0.1560 x + 0.0212 x^2$$

$$c = 11.628 + 0.3340 x + 0.0277 x^2$$

The large difference in ionic radii between S and Te (0.37 Å) prevents formation of solid solutions in the CuInS_{2-x}Te_x system, however, the single alloy CuInS_{1.5}Te_{0.5} has been reported.

6.2.6 Orientation effects

Once single crystals of high purity silicon or gallium arsenide are produced they are cut into wafers such that the exposed face of these wafers is either the crystallographic {100} or {111} planes. The relative structure of these surfaces are important with respect to oxidation, etching and thin film growth. These processes are orientation-sensitive; that is, they depend on the direction in which the crystal slice is cut.

6.2.6.1 Atom density and dangling bonds

The principle planes in a crystal may be differentiated in a number of ways, however, the atom and/or bond density are useful in predicting much of the chemistry of semiconductor surfaces. Since both silicon and gallium arsenide are *fcc* structures and the {100} and {111} are the only technologically relevant surfaces, discussions will be limited to *fcc* {100} and {111}.

The atom density of a surface may be defined as the number of atoms per unit area. Figure 6.22 shows a schematic view of the {111} and {100} planes in a *fcc* lattice. The {111} plane consists of a hexagonal close packed array in which the crystal directions within the plane are oriented at 60° to each other. The hexagonal packing and the orientation of the crystal directions are indicated in Figure 6.22b as an overlaid hexagon. Given the intra-planar inter-atomic distance may be defined as a function of the lattice parameter, the area of this hexagon may be readily calculated. For example in the case of silicon, the hexagon has an area of 38.30 \AA^2 . The number of atoms within the hexagon is three: the atom in the center plus $1/3$ of each of the six atoms at the vertices of the hexagon (each of the atoms at the hexagons vertices is shared by three other adjacent hexagons). Thus, the atom density of the {111} plane is calculated to be 0.0783 \AA^{-2} . Similarly, the atom density of the {100} plane may be calculated. The {100} plane consists of a square array in which the crystal directions within the plane are oriented at 90° to each other. Since the square is coincident with one of the faces of the unit cell the area of the square may be readily calculated. For example in the case of silicon, the square has an area of 29.49 \AA^2 . The number of atoms within the square is 2: the atom in the center plus $1/4$ of each of the four atoms at the vertices of the square (each of the atoms at the corners of the square are shared by four other adjacent squares). Thus, the atom density of the {100} plane is calculated to be 0.0678 \AA^{-2} . While these values for the atom density are specific for silicon, their ratio is constant for all diamond cubic and zinc blende structures: {100}:{111} = 1:1.155. In general, the fewer dangling bonds the more stable a surface structure.

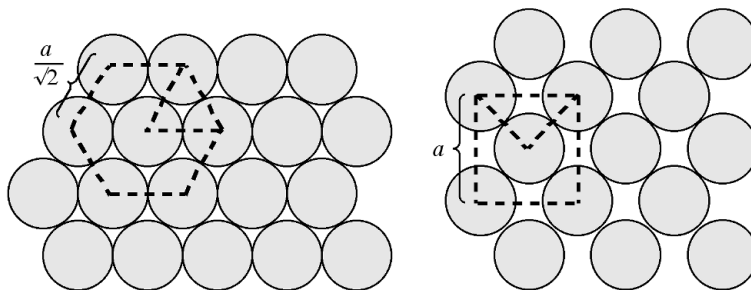


Figure 6.22: Schematic representation of the (111) and (100) faces of a face centered cubic (*fcc*) lattice showing the relationship between the close packed rows.

An atom inside a crystal of any material will have a coordination number (n) determined by the structure of the material. For example, all atoms within the bulk of a silicon crystal will be in a tetrahedral four-coordinate environment ($n = 4$). However, at the surface of a crystal the atoms will not make their full complement of bonds. Each atom will therefore have less nearest neighbors than an atom within the bulk of the material. The missing bonds are commonly called dangling bonds. While this description is not particularly accurate it is, however, widely employed and as such will be used herein. The number of dangling bonds may be defined as the difference between the ideal coordination number (determined by the bulk crystal structure) and the actual coordination number as observed at the surface.

Figure 6.23 shows a section of the {111} surfaces of a diamond cubic lattice viewed perpendicular to the

$\{111\}$ plane. The atoms within the bulk have a coordination number of four. In contrast, the atoms at the surface (e.g., the atom shown in blue in Figure 6.23) are each bonded to just three other atoms (the atoms shown in red in Figure 6.23), thus each surface atom has one dangling bond. As can be seen from Figure 6.24, which shows the atoms at the $\{100\}$ surface viewed perpendicular to the $\{100\}$ plane, each atom at the surface (e.g., the atom shown in blue in Figure 6.24) is only coordinated to two other atoms (the atoms shown in red in Figure 6.24), leaving two dangling bonds per atom. It should be noted that the same number of dangling bonds are found for the $\{111\}$ and $\{100\}$ planes of a zinc blende lattice. The ratio of dangling bonds for the $\{100\}$ and $\{111\}$ planes of all diamond cubic and zinc blende structures is $\{100\}:\{111\} = 2:1$. Furthermore, since the atom densities of each plane are known then the ratio of the dangling bond densities is determined to be: $\{100\}:\{111\} = 1:0.577$.

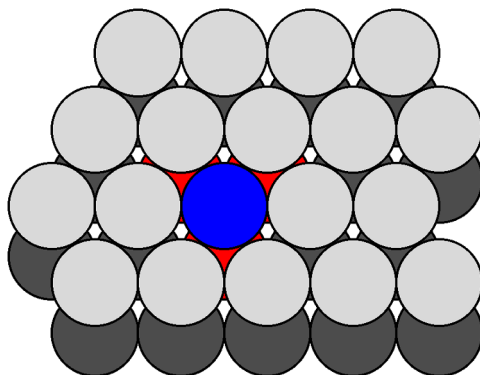


Figure 6.23: A section of the $\{111\}$ surfaces of a diamond cubic lattice viewed perpendicular to the $\{111\}$ plane.

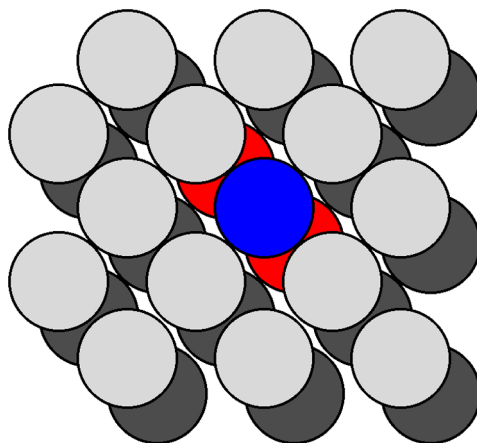


Figure 6.24: A section of the $\{100\}$ surface of a diamond cubic lattice viewed perpendicular to the $\{100\}$ plane.

6.2.6.2 Silicon

For silicon, the $\{111\}$ planes are closer packed than the $\{100\}$ planes. As a result, growth of a silicon crystal is therefore slowest in the $\langle 111 \rangle$ direction, since it requires laying down a close packed atomic layer upon another layer in its closest packed form. As a consequence $\langle 111 \rangle$ Si is the easiest to grow, and therefore the least expensive.

The dissolution or etching of a crystal is related to the number of broken bonds already present at the surface: the fewer bonds to be broken in order to remove an individual atom from a crystal, the easier it will be to dissolve the crystal. As a consequence of having only one dangling bond (requiring three bonds to be broken) etching silicon is slowest in the $\langle 111 \rangle$ direction. The electronic properties of a silicon wafer are also related to the number of dangling bonds.

Silicon microcircuits are generally formed on a single crystal wafer that is diced after fabrication by either sawing part way through the wafer thickness or scoring (scribing) the surface, and then physically breaking. The physical breakage of the wafer occurs along the natural cleavage planes, which in the case of silicon are the $\{111\}$ planes.

6.2.6.3 Gallium arsenide

The zinc blende lattice observed for gallium arsenide results in additional considerations over that of silicon. Although the $\{100\}$ plane of GaAs is structurally similar to that of silicon, two possibilities exist: a face consisting of either all gallium atoms or all arsenic atoms. In either case the surface atoms have two dangling bonds, and the properties of the face are independent of whether the face is gallium or arsenic.

The $\{111\}$ plane also has the possibility of consisting of all gallium or all arsenic. However, unlike the $\{100\}$ planes there is a significant difference between the two possibilities. Figure 6.17 shows the gallium arsenide structure represented by two interpenetrating *fcc* lattices. The $[111]$ axis is vertical within the plane of the page. Although the structure consists of alternate layers of gallium and arsenic stacked along the $[111]$ axis, the distance between the successive layers alternates between large and small. Assigning arsenic as the parent lattice the order of the layers in the $[111]$ direction is As-Ga-As-Ga-As-Ga, while in the $\left[\begin{smallmatrix} - \\ - \\ - \end{smallmatrix} \right]$

direction the layers are ordered, Ga-As-Ga-As-Ga-As (Figure 6.25). In silicon these two directions are of course identical. The surface of a crystal would be either arsenic, with three dangling bonds, or gallium, with one dangling bond. Clearly, the latter is energetically more favorable. Thus, the (111) plane shown in Figure 6.25 is called the (111) Ga face. Conversely, the $\left[\bar{1}\bar{1}\bar{1}\right]$ plane would be either gallium, with three dangling bonds, or arsenic, with one dangling bond. Again, the latter is energetically more favorable and the $\left[\bar{1}\bar{1}\bar{1}\right]$ plane is therefore called the (111) As face.

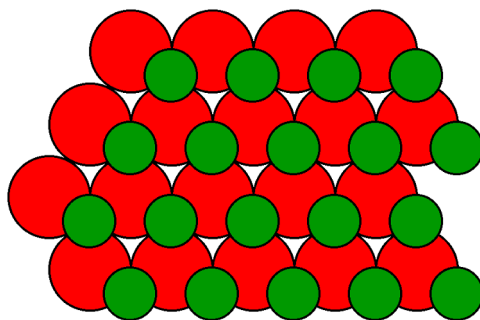


Figure 6.25: The (111) Ga face of GaAs showing a surface layer containing gallium atoms (green) with one dangling bond per gallium and three bonds to the arsenic atoms (red) in the lower layer.

The (111) As is distinct from that of (111) Ga due to the difference in the number of electrons at the surface. As a consequence, the (111) As face etches more rapidly than the (111) Ga face. In addition, surface evaporation below 770 °C occurs more rapidly at the (111) As face.

6.2.7 Bibliography

- M. Baublitz and A. L. Ruoff, *J. Appl. Phys.*, 1982, **53**, 6179.
- J. C. Jamieson, *Science*, 1963, **139**, 845.
- C. C. Landry, J. Lockwood, and A. R. Barron, *Chem. Mater.*, 1995, **7**, 699.
- M. Robbins, J. C. Phillips, and V. G. Lambrecht, *J. Phys. Chem. Solids*, 1973, **34**, 1205.
- D. Sridevi and K. V. Reddy, *Mat. Res. Bull.*, 1985, **20**, 929.
- Y. K. Vohra, S. T. Weir, and A. L. Ruoff, *Phys. Rev. B*, 1985, **31**, 7344.
- W. M. Yin and R. J. Paff, *J. Appl. Phys.*, 1973, **45**, 1456.

6.3 X-ray Crystallography

6.3.1 An Introduction to X-ray Diffraction³

6.3.1.1 History of X-ray crystallography

The birth of X-ray crystallography is considered by many to be marked by the formulation of the *law of constant angles* by Nicolaus Steno in 1669 (Figure 6.26). Although Steno is well known for his numerous

³This content is available online at <<http://cnx.org/content/m38289/1.2/>>.

principles regarding all areas of life, this particular law dealing with geometric shapes and crystal lattices is familiar ground to all chemists. It simply states that *the angles between corresponding faces on crystals are the same for all specimens of the same mineral*. The significance of this for chemistry is that given this fact, crystalline solids will be easily identifiable once a database has been established. Much like solving a puzzle, crystal structures of heterogeneous compounds could be solved very methodically by comparison of chemical composition and their interactions.



Figure 6.26: Danish pioneer in both anatomy and geology Nicolas Steno (1638 – 1686).

Although Steno was given credit for the notion of crystallography, the man that provided the tools necessary to bring crystallography into the scientific arena was Wilhelm Roentgen (Figure 6.27), who in 1895 successfully pioneered a new form of photography, one that could allegedly penetrate through paper, wood, and human flesh; due to a lack of knowledge of the specific workings of this new discovery, the scientific community conveniently labeled the new particles *X-rays*. This event set off a chain reaction of experiments and studies, not all performed by physicists. Within one single month, medical doctors were using X-rays to pinpoint foreign objects such in the human body such as bullets and kidney stones (Figure 6.28).



Figure 6.27: German physicist Wilhelm Conrad Röntgen (1845 – 1923).



Figure 6.28: First public X-ray image ever produced. Pictured is the left hand of Anna Berthe Röntgen. The uncharacteristic bulge is her ring.

The credit for the actual discovery of X-ray diffraction goes to Max von Laue (Figure 6.29), to whom the Nobel Prize in physics in 1914 was awarded for the discovery of the diffraction of X-rays. Legend has it that the notion that eventually led to a Nobel prize was born in a garden in Munich, while von Laue was pondering the problem of passing waves of electromagnetic radiation through a specific crystalline arrangement of atoms. Because of the relatively large wavelength of visible light, von Laue was forced to turn his attention to another part of the electromagnetic spectrum, to where shorter wavelengths resided. Only a few decades earlier, Röntgen had publicly announced the discovery of X-rays, which supposedly had a wavelength shorter than that of visible light. Having this information, von Laue entrusted the task of performing the experimental work to two technicians, Walter Friedrich and Paul Knipping. The setup consisted of an X-ray source, which beamed radiation directly into a copper sulfate crystal housed in a lead box. Film was lined against the sides and back of the box, so as to capture the X-ray beam and its diffraction pattern. Development of the film showed a dark circle in the center of the film, surrounded by several extremely well defined circles, which had formed as a result of the diffraction of the X-ray beam by the ordered geometric arrangement of copper sulfate. Max von Laue then proceeded to work out the mathematical formulas involved in the observed diffraction pattern, for which he was awarded the Nobel Prize in physics in 1914.



Figure 6.29: German physicist Max Theodor Felix von Laue (1879 – 1960) won the Nobel Prize for discovery of the diffraction of X-rays by crystals.

6.3.1.2 Principles of X-ray diffraction (XRD)

The simplest definition of diffraction is *the irregularities caused when waves encounter an object*. Diffraction is a phenomenon that exists commonly in everyday activities, but is often disregarded and taken for granted. For example, when looking at the information side of a compact disc, a rainbow pattern will often appear when it catches light at a certain angle. This is caused by visible light striking the grooves of the disc, thus producing a rainbow effect (Figure 6.30), as interpreted by the observers' eyes. Another example is the formation of seemingly concentric rings around an astronomical object of significant luminosity when

observed through clouds. The particles that make up the clouds diffract light from the astronomical object around its edges, causing the illusion of rings of light around the source. It is easy to forget that diffraction is a phenomenon that applies to all forms of waves, not just electromagnetic radiation. Due to the large variety of possible types of diffractions, many terms have been coined to differentiate between specific types. The most prevalent type of diffraction to X-ray crystallography is known as Bragg diffraction, which is defined as the scattering of waves from a crystalline structure.



Figure 6.30: The rainbow effects caused by visible light striking the grooves of a compact disc (CD).

Formulated by William Lawrence Bragg (Figure 6.31), the equation of Bragg's law relates wavelength to angle of incidence and lattice spacing, (6.10), where n is a numeric constant known as the order of the diffracted beam, λ is the wavelength of the beam, d denotes the distance between lattice planes, and θ represents the angle of the diffracted wave. The conditions given by this equation must be fulfilled if diffraction is to occur.

$$n\lambda = 2d \sin(\theta) \tag{6.10}$$

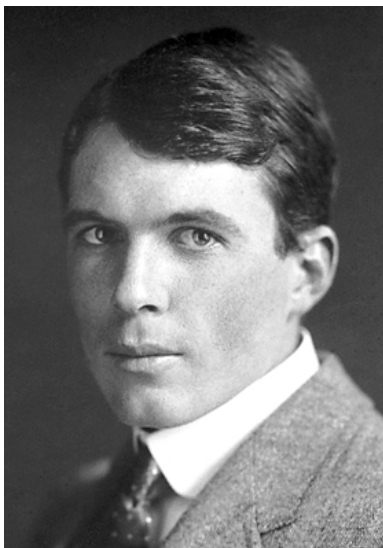


Figure 6.31: Australian-born British physicist Sir William Lawrence Bragg (1890 – 1971).

Because of the nature of diffraction, waves will experience either constructive (Figure 6.32) or destructive (Figure 6.33) interference with other waves. In the same way, when an X-ray beam is diffracted off a crystal, the different parts of the diffracted beam will have seemingly stronger energy, while other parts will have seemed to lost energy. This is dependent mostly on the wavelength of the incident beam, and the spacing between crystal lattices of the sample. Information about the lattice structure is obtained by varying beam wavelengths, incident angles, and crystal orientation. Much like solving a puzzle, a three dimensional structure of the crystalline solid can be constructed by observing changes in data with variation of the aforementioned variables

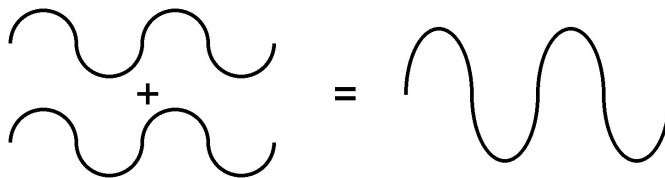


Figure 6.32: Schematic representation of constructive interference.

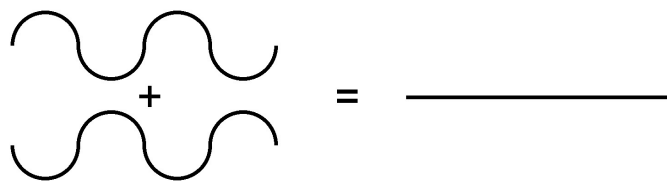


Figure 6.33: Schematic representation of destructive interference.

6.3.1.3 The X-ray diffractometer

At the heart of any XRD machine is the X-ray source. Modern day machines generally rely on copper metal as the element of choice for producing X-rays, although there are variations among different manufacturers. Because diffraction patterns are recorded over an extended period of time during sample analysis, it is very important that beam intensity remain constant throughout the entire analysis, or else faulty data will be procured. In light of this, even before an X-ray beam is generated, current must pass through a voltage regular, which will guarantee a steady stream of voltage to the X-ray source.

Another crucial component to the analysis of crystalline via X-rays is the detector. When XRD was first developed, film was the most commonly used method for recognizing diffraction patterns. The most obvious disadvantage to using film is the fact that it has to be replaced every time a new specimen is introduced, making data collection a time consuming process. Furthermore, film can only be used once, leading to an increase in cost of operating diffraction analysis.

Since the origins of XRD, detection methods have progressed to the point where modern XRD machines are equipped with semiconductor detectors, which produce pulses proportional to the energy absorbed. With these modern detectors, there are two general ways in which a diffraction pattern may be obtained. The first is called continuous scan, and it is exactly what the name implies. The detector is set in a circular motion around the sample, while a beam of X-ray is constantly shot into the sample. Pulses of energy are plotted with respect to diffraction angle, which ensure all diffracted X-rays are recorded. The second and more widely used method is known as step scan. Step scanning bears similarity to continuous scan, except it is highly computerized and much more efficient. Instead of moving the detector in a circle around the entire sample, step scanning involves collecting data at one fixed angle at a time, thus the name. Within these detection parameters, the types of detectors can themselves be varied. A more common type of detector, known as the charge-coupled device (CCD) detector (Figure 6.34), can be found in many XRD machines, due to its fast data collection capability. A CCD detector is comprised of numerous radiation sensitive grids, each linked to sensors that measure changes in electromagnetic radiation. Another commonly seen type of detector is a simple scintillation counter (Figure 6.35), which counts the intensity of X-rays that it encounters as it moves along a rotation axis. A comparable analogy to the differences between the two detectors mentioned would be that the CCD detector is able to see in two dimensions, while scintillation counters are only able to see in one dimension.



Figure 6.34: Single crystal X-ray diffractometer with a CCD detector. The incident beam is generated and delivered through the silver apparatus on the right side of the sample, and the detector is the large black camera to the left of the sample.

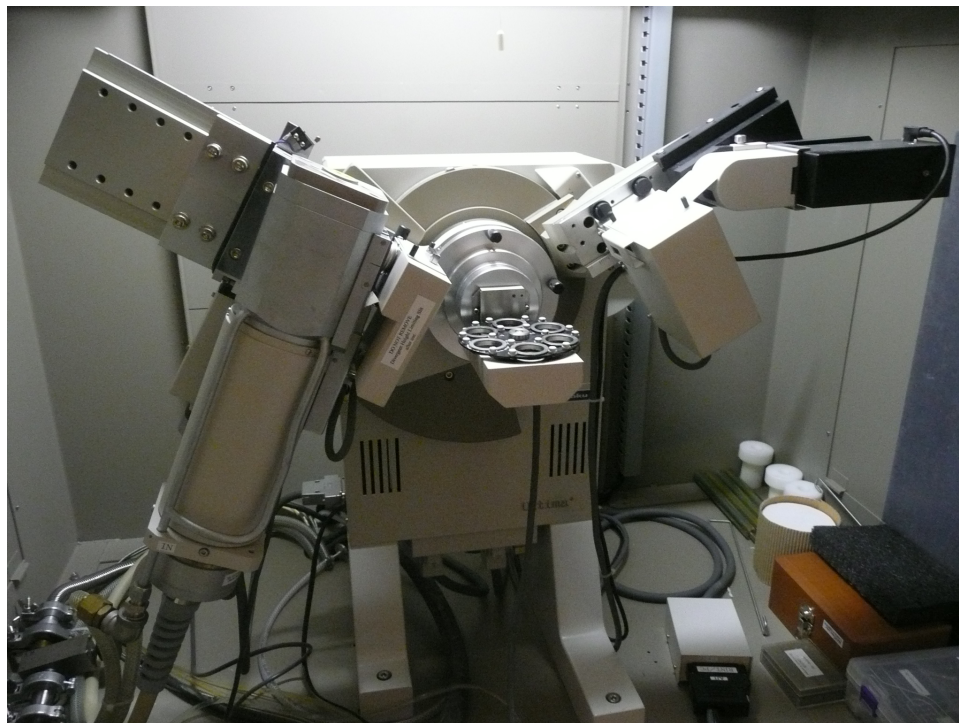


Figure 6.35: Image of a powder X-ray diffractometer. The incident beam enters from the tube on the left, and the detector is housed in the black box on the right side of the machine. This particular XRD machine is capable of handling six samples at once, and is fully automated from sample to sample.

Aside from the above two components, there are many other variables involved in sample analysis by an XRD machine. As mentioned earlier, a steady incident beam is extremely important for good data collection. To further ensure this, there will often be what is known as a Söller slit or collimator found in many XRD machines. A Söller slit collimates the direction of the X-ray beam. In the collimated X-ray beam the rays are parallel, and therefore will spread minimally as they propagate (Figure 6.36). Without a collimator X-rays from all directions will be recorded; for example, a ray that has passed through the top of the specimen (see the red arrow in Figure 6.36a) but happens to be traveling in a downwards direction may be recorded at the bottom of the plate. The resultant image will be so blurred and indistinct as to be useless. Some machines have a Söller slit between the sample and the detector, which drastically reduces the amount of background noise, especially when analyzing iron samples with a copper X-ray source.

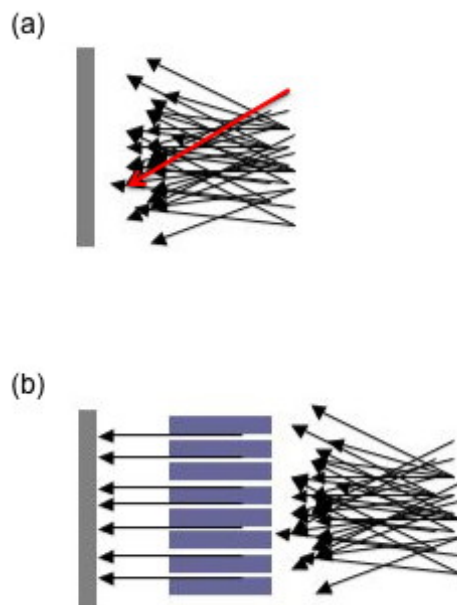


Figure 6.36: How a Söller collimator filters a stream of rays. (a) without a collimator and (b) with a collimator.

This single crystal XRD machine (Figure 6.34) features a cooling gas line, which allows the user to bring down the temperature of a sample considerably below room temperature. Doing so allows for the opportunities for studies performed where the sample is kept in a state of extremely low energy, negating a lot of vibrational motion that might interfere with consistent data collection of diffraction patterns. Furthermore, information can be collected on the effects of temperature on a crystal structure. Also seen in Figure 6.34 is the hook-shaped object located between the beam emitter and detector. It serves the purpose of blocking X-rays that were not diffracted from being seen by the detector, drastically reducing the amount of unnecessary noise that would otherwise obscure data analysis.

6.3.1.4 Evolution of powder XRD

Over time, XRD analysis has evolved from a very narrow and specific field to something that encompasses a much wider branch of the scientific arena. In its early stages, XRD was (with the exception of the simplest structures) confined to single crystal analysis, as detection methods had not advanced to a point where more complicated procedures were able to be performed. After many years of discovery and refining, however, technology has progressed to where crystalline properties (structure) of solids can be gleaned directly from a powder sample, thus offering information for samples that cannot be obtained as a single crystal. One area in which this is particularly useful is pharmaceuticals, since many of the compounds studied are not available in single crystal form, only in a powder.

Even though single crystal diffraction and powder diffraction essentially generate the same data, due to the powdered nature of the latter sample, diffraction lines will often overlap and interfere with data collection. This is apparently especially when the diffraction angle 2θ is high; patterns that emerge will be almost to the point of unidentifiable, because of disruption of individual diffraction patterns. For this particular reason, a new approach to interpreting powder diffraction data has been created.

There are two main methods for interpreting diffraction data:

- The first is known as the traditional method, which is very straightforward, and bears resemblance to single crystal data analysis. This method involves a two step process: 1) the intensities and diffraction patterns from the sample is collected, and 2) the data is analyzed to produce a crystalline structure. As mentioned before, however, data from a powdered sample is often obscured by multiple diffraction patterns, which decreases the chance that the generated structure is correct.
- The second method is called the direct-space approach. This method takes advantage of the fact that with current technology, diffraction data can be calculated for any molecule, whether or not it is the molecule in question. Even before the actual diffraction data is collected, a large number of theoretical patterns of suspect molecules are generated by computer, and compared to experimental data. Based on correlation and how well the theoretical pattern fits the experimental data best, a guess is formulated to which compound is under question. This method has been taken a step further to mimic social interactions in a community. For example, first generation theoretical trial molecules, after comparison with the experimental data, are allowed to evolve within parameters set by researchers. Furthermore, if appropriate, molecules are produce offspring with other molecules, giving rise to a second generation of molecules, which fit the experimental data even better. Just like a natural environment, genetic mutations and natural selection are all introduced into the picture, ultimately giving rise a molecular structure that represents data collected from XRD analysis.

Another important aspect of being able to study compounds in powder form for the pharmaceutical researcher is the ability to identify structures in their natural state. A vast majority of drugs in this day and age are delivered through powdered form, either in the form of a pill or a capsule. Crystallization processes may often alter the chemical composition of the molecule (e.g., by the inclusion of solvent molecules), and thus marring the data if confined to single crystal analysis. Furthermore, when the sample is in powdered form, there are other variables that can be adjusted to see real-time effects on the molecule. Temperature, pressure, and humidity are all factors that can be changed in-situ to glean data on how a drug might respond to changes in those particular variables.

6.3.1.5 Bibliography

- H. D. Jakubke and H. Jeschkeit, *Concise Encyclopedia Chemistry*, Walter de Gruyter, Berlin (1993).
- M. von Laue, *Concerning the detection of X-ray interferences*, Nobel Prize. Nobel Foundation (1915).
- K. Harris, *Am. Pharmaceut. Rev.*, 2004, **7.2**, 86.
- B. D. Cullity and S. R. Stock. *Elements of X-ray Diffraction*, 3rd Edition, Prentice Hall, New Jersey (2001).

6.3.2 Powder X-Ray Diffraction⁴

6.3.2.1 Introduction

Powder X-Ray diffraction (XRD) was developed in 1916 by Debye (Figure 6.37) and Scherrer (Figure 6.38) as a technique that could be applied where traditional single-crystal diffraction cannot be performed. This includes cases where the sample cannot be prepared as a single crystal of sufficient size and quality. Powder samples are easier to prepare, and is especially useful for pharmaceuticals research.

⁴This content is available online at <<http://cnx.org/content/m46152/1.2/>>.



Figure 6.37: Dutch physicist and physical chemist Peter Joseph William Debye (1884-1966) recipient of the Nobel Prize in Chemistry.



Figure 6.38: Swiss physicist Paul Scherrer (1890-1969).

Diffraction occurs when a wave meets a set of regularly spaced scattering objects, and its wavelength of the distance between the scattering objects are of the same order of magnitude. This makes X-rays suitable for crystallography, as its wavelength and crystal lattice parameters are both in the scale of angstroms (\AA). Crystal diffraction can be described by Bragg diffraction, (6.11), where λ is the wavelength of the incident

monochromatic X-ray, d is the distance between parallel crystal planes, and θ the angle between the beam and the plane.

$$\lambda = 2d \sin\theta \quad (6.11)$$

For constructive interference to occur between two waves, the path length difference between the waves must be an integral multiple of their wavelength. This path length difference is represented by $2d \sin\theta$ Figure 6.39. Because $\sin\theta$ cannot be greater than 1, the wavelength of the X-ray limits the number of diffraction peaks that can appear.

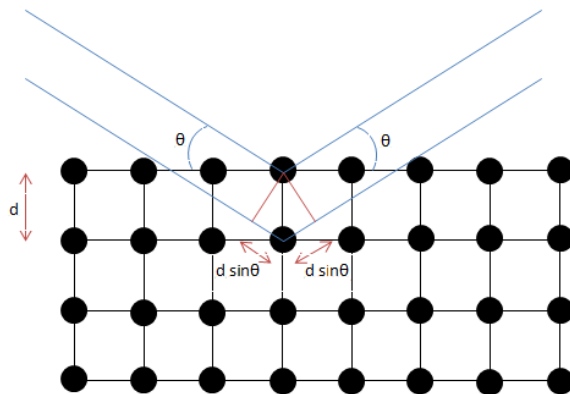


Figure 6.39: Bragg diffraction in a crystal. The angles at which diffraction occurs is a function of the distance between planes and the X-ray wavelength.

6.3.2.2 Production and detection of X-rays

Most diffractometers use Cu or Mo as an X-ray source, and specifically the K_{α} radiation of wavelengths of 1.54059 \AA and 0.70932 \AA , respectively. A stream of electrons is accelerated towards the metal target anode from a tungsten cathode, with a potential difference of about 30-50 kV. As this generates a lot of heat, the target anode must be cooled to prevent melting.

Detection of the diffracted beam can be done in many ways, and one common system is the gas proportional counter (GPC). The detector is filled with an inert gas such as argon, and electron-ion pairs are created when X-rays pass through it. An applied potential difference separates the pairs and generates secondary ionizations through an avalanche effect. The amplification of the signal is necessary as the intensity of the diffracted beam is very low compared to the incident beam. The current detected is then proportional to the intensity of the diffracted beam. A GPC has a very low noise background, which makes it widely used in labs.

6.3.2.3 Performing X-ray diffraction

WARNING: Exposure to X-rays may have health consequences, follow safety procedures when using the diffractometer.

The particle size distribution should be even to ensure that the diffraction pattern is not dominated by a few large particles near the surface. This can be done by grinding the sample to reduce the average particle size to $<10\mu\text{m}$. However, if particle sizes are too small, this can lead to broadening of peaks. This is due to both lattice damage and the reduction of the number of planes that cause destructive interference.